Batteries & Supercaps

Research Article
doi.org/10.1002/batt.202500485

Chemistry Europe
European Chemical Societies Publishing

www.batteries-supercaps.org

Multitype Interaction Between a Redox-Active Inclusion Complex, Polymer, and Polysulfides that Boosts the Performance of Lithium–Sulfur Batteries

Marimuthu Senthilkumaran, Bharathkumar H. Javaregowda, Tejas Rajput, Kadhiravan Shanmuganathan, Prakashbabu Rajendran,* Debmalya Roy,* and Kothandam Krishnamoorthy*

Polysulfides formed in Li–S batteries pose various characteristics. For example, Li_2S is solid while Li_2S_4 is liquid. Li_2S is insoluble in battery electrolytes while Li_2S_4 is soluble. All of them are negative charge bearing molecules. Lithium polysulfides are Lewis acids. Herein, a binder with multiple interaction motifs is presented to confine the polysulfides in the cathode. The base of the binder is sodium salt of carboxy methyl cellulose (CMC). β-cyclodextrin (CD) that comprises 21 hydroxyl groups is used because they hydrogen bond with the carboxylate moieties of CMC to impart mechanical strength to the binder to accommodate volume change during the sulfur to polysulfide conversion. Indeed, it is found that the binder with CD shows improved mechanical properties compared to CMC. The cavity of the CD is used to prepare an inclusion complex with ferrocene methanol. Due to the presence of Fe^{2+}, the batteries comprising the inclusion complex show improved electrocatalytic properties. The Li–S batteries deliver a specific capacity of 780 mA h g^{-1} (1 C) at a high sulfur loading of 4.7 mg cm^{-2} and lean electrolyte (E/S of 5 μL mg^{-1}).

1. Introduction

Lithium sulfur batteries (LSBs) are attractive due to their high theoretical specific capacity and energy density. Furthermore, sulfur is abundantly available at petroleum refineries, which is another attractive aspect. Nevertheless, the commercialization of LSBs remains a challenge due to several factors.[1,2] The major challenges from the sulfur cathode side are; 1) the insulating nature of sulfur and it's discharged products, especially Li_2S_2 and Li_2S, 2) the shuttle effect of the soluble lithium polysulfides (LiPSs) such as Li_2S_8, Li_2S_6, and Li_2S_4, and 3) the large volume change from the reactant S to final product Li_2S, leading to rapid capacity degradation, low Coulombic efficiency, and active material loss.[3–5] On the lithium anode side, due to the high chemical reactivity of metallic lithium, dendrite formation is hard to avoid, which causes short circuits and affects the battery safety. The reaction between LiPSs with metallic lithium forms an unstable solid-electrolyte interface (SEI) layer, and results in electrolyte decomposition and rapid anode degradation.[6–8] To address these problems, many strategies have been developed. Design and synthesis of sulfur hosts,[9–11] modification of the separator[12,13] and electrolyte additives[14,15] is some of the widely explored approaches. The sulfur hosts are mixed with a binder and conducting carbon to prepare the LSBs cathode. The widely used binder in all types of rechargeable batteries is PVDF.[16]

PVDF is also used in LSBs that do not have any specific interaction with either sulfur or polysulfides.[17] Synthesis of any fluoro compound is challenging, which is true in case of PVDF as well.[18] The PVDF is dissolved in N-methyl-2-pyrrolidone (NMP) to prepare a cathode film for LSBs; however, efforts are on to avoid NMP due to the issues associated with it.[19] In recent years, biopolymer-based binders have been explored in fabricating mechanically robust or expansion tolerable sulfur cathodes.[20] Among them, carboxymethyl cellulose (CMC) is a low-cost water processable polymer that comprises abundant carboxylic (—COOH) and hydroxyl (—OH) functional groups, which is beneficial for making a homogeneous slurry.[21] The combination of a CMC binder and a porous carbon paper current collector delivered an initial capacity of 1180 mA h g^{-1} at 0.02 C and a retained capacity of 860 mA h g^{-1} after 50 cycles at 0.02 C with a sulfur loading of 4 mg cm^{-2}.[22] Coin cells with a sulfur loading of 6 mg cm^{-2} using CMC binder, which exhibited a capacity of around 1000 mA hg^{-1} at 0.2 C after 100 cycles.[23] CMC-styrene butadiene rubber hybrid binder exhibited improved performance. They showed high-rate capability (≈800 mA h g^{-1} at 6.0 C) and long cycling performance up to 1500 cycles with 0.039% decay per cycle.[24] Similarly, sulfur

M. Senthilkumaran, B. H. Javaregowda, T. Rajput, K. Shanmuganathan, P. Rajendran, K. Krishnamoorthy
Polymer Science and Engineering Division
CSIR-National Chemical Laboratory
Dr. Homi Bhabha Road, Pune, Maharashtra 411008, India
E-mail: prakashumass2011@gmail.com
k.krishnamoorthy@ncl.res.in

B. H. Javaregowda, T. Rajput, K. Shanmuganathan, K. Krishnamoorthy
Academy of Scientific and Innovative Research
Ghaziabad, Uttar Pradesh 200102, India

D. Roy
DRDO- Defence Materials and Stores Research and Development Establishment
Kanpur, Uttar Pradesh 208013, India
E-mail: droy.dmsrde@gov.in

Supporting information for this article is available on the WWW under https://doi.org/10.1002/batt.202500485

Research Article
doi.org/10.1002/batt.202500485
Chemistry Europe
European Chemical Societies Publishing

cathode with a loading of 4.5 mg cm^{-2} using the CMC-NBR binder delivered ≈350 mA h g^{-1} at 0.2 C after 100 cycles.[25] CMC-glucose-based binder system suppressed polysulfides shuttle significantly. During casting, the above binder system provided the sulfur cathode with a desirable web-like microstructure. This cathode exhibited a capacity of 700 mA h g^{-1} at 0.2 C for 1000 cycles at a 3 mg cm^{-2} sulfur loading, but no obvious capacity improvement was observed for thick cathodes (loading of >5 mg cm^{-2}), coated in coin or pouch cell configurations.[26] CMC-PVP-I redox binder system delivers high specific capacities at even high C rates (1 and 2 C) under practical sulfur loading (3–7 mg cm^{-2}) conditions.[27] Apart from this, electrocatalyst's role in LSBs is an important factor to enhance the amount of sulfur consumption, thereby improving the overall LSBs electrochemical performance. Accelerating the reaction kinetics of the LSBs chemistry using iodide/triiodide (I^-/I^{3-}) redox couple,[28] ferrocene (Fc) and anthraquinone[29] and cobalt/nickel phthalocyanine is well reported in the literature.[30,31]

By considering the above facts, we have chosen the sodium salt of CMC as a binder. The CMC is mixed with β-cyclodextrin (CD), which is chosen for the following reasons, 1) it has 21 hydroxyl groups compared to five in glucose, 2) the hydroxyl groups can form hydrogen bonding network with carboxylic acid functionalities of CMC improving the mechanical stability of the binder, and 3) the cavity can be used to form an inclusion complex unlike glucose. Indeed, we formed an inclusion complex with ferrocene methanol (FcOH). The hydroxyl moiety of FcOH can also form hydrogen bonding with the CMC. We hypothesized that the five-membered ring without the substitution will be inserted into the cavity of CD, leaving Fe^{2+} and cyclopentadiene with -CH_2OH outside the cavity (**Scheme 1**). The Fe^{2+} is a Lewis acid that can interact with Lewis basic polysulfides, suppressing polysulfide dissolution. Recently, we have shown that the Ni^{2+} can electro catalyze sulfur redox reaction while electrostatically attracting polysulfides. Therefore, we have prepared S/C composite with nickel(II)phthalocyanine (NPT).[30] Due to multitype interaction that was imparted to the electrode, the polysulfide shuttle is effectively suppressed, and sulfur redox reaction was catalyzed. This binder will be mentioned as the CMC-CD-FcOH in all further discussions. As a control, CMC and CD (CMC-CD) blend has also been tested, which showed inferior performance compared to CMC-CD-FcOH binder. This indicates the necessity to use FcOH inclusion complex. Overall, the CMC-CD-FcOH fulfills the necessary criterion to realize electrochemically stable LSBs. When employing CMC-CD-FcOH binder, the LSBs displayed a high specific capacity of 1100 mA h g^{-1} at 0.2 C with 89% capacity retention after 120 cycles. On the other hand, the control sample without FcOH could retain 72% of its initial capacity after 120 cycles. Furthermore, the LSBs with CMC-CD-FcOH delivered a high specific capacity of 1035 mA h g^{-1} at 0.5 C with ≈75% capacity retention after 500 cycles. The LSBs with this binder at higher S loading of 3.5 and 4.7 mg cm^{-2} with E/S ratio of 5 μL mg^{-1} delivered 900 and 780 mA h g^{-1} at 1 C.

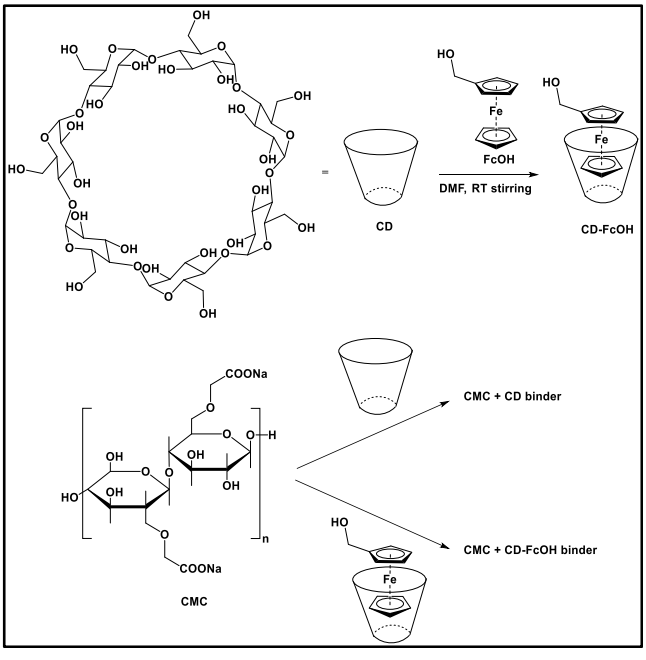

Scheme 1. The preparation route of CMC-CD and CMC-CD-FcOH.

2. Results and Discussion

The inclusion complex between CD and Fc-OH was prepared by following the reported procedure.[32] The inclusion complex between CD and Fc-OH was studied by 1H NMR spectroscopy and the spectrum is given in (Figure S1, Supporting Information). The 2D nuclear overhauser effect spectroscopy NMR peaks corresponding to ferrocene at $\delta = 4.17$–4.55 ppm are in resonance with the signals of the CD cavity protons at $\delta = 3.55$–3.80 ppm (Figure S2, Supporting Information). The proximity of the CD and ferrocene units thus confirms the formation of the host–guest inclusion complex. The inclusion complex will be mentioned as CD-FcOH. The blend of this complex with CMC will be mentioned as CMC-CD-FcOH. The scheme for the preparation of CMC-CD and CMC-CD-FcOH is provided in Scheme 1. Polysulfide adsorption tests were conducted to understand the interaction between either CMC-CD-FcOH or CMC-CD and polysulfides. For this test, either CMC-CD-FcOH or CMC-CD was dispersed in Li_2S_8 solution. The photographs of sample vials comprising Li_2S_8 and the binders are shown **Figure 1**a. In case of CMC-CD-FcOH complete discoloration of Li_2S_8 was observed corroborating strong adsorption of polysulfides with the Fe^{2+} and hydroxyl groups of CMC and CD. On the other hand, the solution comprising CMC-CD displayed pale yellow colored solution indicating a moderate adsorption. This is due to the absence of Lewis acidic Fe^{2+} in CMC-CD.

UV–vis. absorption spectra of the solutions were recorded to study the change in adsorption of Li_2S_8 upon addition of either CMC-CD-FcOH or CMC-CD. The Li_2S_8 solution displayed peaks at 260 (S_8), 300 (S_6^{2-}), 375 (S_4^{2-}), and 440 nm (S_8^{2-}).[33] The absorbance intensity of these peaks was reduced for the solution comprising CMC-CD and CMC-CD-FcOH (Figure 1b). However, the decrease in intensity was more pronounced in the case of CMC-CD-FcOH, indicating stronger polysulfide adsorption due to multitype attractive

Research Article
doi.org/10.1002/batt.202500485
Chemistry Europe
European Chemical Societies Publishing

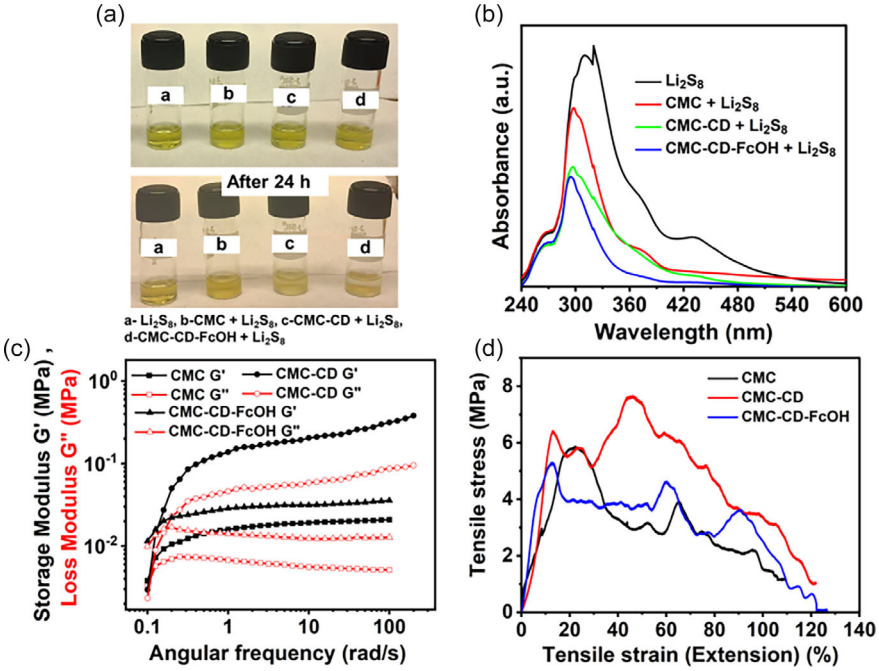

Figure 1. a) Picture showing the polysulfide adsorption behavior of the binders, b) UV–vis. absorption spectrum of Li_2S_8, Li_2S_8 + CMC, Li_2S_8 + CMC-CD, and Li_2S_8 + CMC-CD-FcOH, c) plot showing the variation of storage and loss modulus as a function of angular frequency for the electrode slurry with CMC, CMC-CD, and CMC-CD-FcOH, and d) peel off test data for the electrode films comprising CMC, CMC-CD, and CMC-CD-FcOH.

interaction. In the next set of experiments, C/S/NPT composite was prepared by melt diffusion strategy, and the sulfur loading was quantified using thermogravimetric analysis (TGA). The sulfur loading was found to be 60% (Figure S3, Supporting Information).

The slurry formulations with CMC, CMC-CD, and CMC-CD-FcOH showed shear thinning behavior with an increase in angular frequency. However, the viscosity (Figure S4, Supporting Information) and the modulus (Figure 1c) found to be the highest for CMC-CD, followed by CMC-CD-FcOH and CMC. We attribute this to the stronger hydrogen bonding interactions between CMC and CD. We anticipate that this hydrogen bonding network could reduce stress and help to buffer the volume expansion. On the other hand, in the case of CMC-CD-FcOH complex, the steric crowding due to the presence of Fc moieties decreases the interaction between CMC and CD. Furthermore, to understand the adhesion properties of the binders and the C/S/NPT composite, the 180° peel off test of the electrode films were carried out. From the stress–strain plot, the electrode films comprising CMC-CD displayed higher strength (64.3 MPa) compared to CMC-CD-FcOH (25.3 MPa) and CMC (50.6 MPa) (Figure 1d) which is in alignment with the rheological data. These observations also align with some of the modeling studies on interfacial adhesion in battery electrodes.[34–36]

In the LSBs, the cathode comprises C/S/NPT composite and CMC-CD-FcOH binder while the Li foil acts as counter and reference electrode. In the control experiments, CMC-CD was the binder instead of CMC-CD-FcOH. Initially, the LSBs were cycled between 1.7 and 2.8 V versus. Li/Li^+. The cyclic voltammograms of LSBs with CMC-CD-FcOH displayed a typical two-step sulfur reduction process with reduction peaks centered at 2.34 and 2.05 V, depicting the conversion of S_8 to Li_2S_z($8 \leq z \leq 4$) and Li_2S_2/Li_2S, respectively (**Figure 2**a). During the anodic scan, two peaks at 2.35 and 2.42 V corresponds to the conversion of Li_2S to polysulfides and S8, respectively. On the other hand, the cell comprising CMC-CD displayed reduction peaks at 2.3 and 1.95 V and a single peak centered at 2.4 V during the anodic scan (Figure 2a). Furthermore, the CV profile of LSBs with CMC-CD-FcOH displayed stable cycling up to five cycles (Figure 2b). Notably, the LSBs with CMC-CD-FcOH displayed lower onset voltage for sulfur reduction (2.37 and 2.05 V vs. 2.3 and 1.98 V) and sulfur evolution reactions (2.25 V vs. 2.3 V) compared to that of CMC-CD. This indicates faster polysulfide conversion kinetics on CMC-CD-FcOH due to the presence of redox active Fc moieties, which catalyze the sulfur to polysulfide conversion (Figure 2c). This observation was further supported by the Tafel slopes. The Tafel slopes for LSBs with CMC-CD-FcOH were estimated to be 30 and 97 mV dec^{-1}, while they are 36 and 100 mV dec^{-1} for CMC-CD (Figure 2d and Figure S5, Supporting Information). Thus, there is an additive effect due to the presence of Ni^{2+} in addition to ferrocene in case of CMC-CD-FcOH.

The CVs at different scan rates were also recorded to understand the Li-ion diffusion kinetics. From the CV of CMC-CD-FcOH, it is evident that the sulfur to polysulfides electrocatalysis is maintained at different scan rates from 0.1 to 0.5 mV s^{-1} (Figure S6, Supporting Information). On the other hand, the CV of CMC-CD at different scan rates showed a single oxidation peak during the anodic scan, indicating poor electrocatalytic activity toward polysulfide conversion (Figure S7, Supporting Information). Next, the LSBs with these binders were subjected to rate performance at different C rates. The LSBs with CMC-CD-FcOH binder delivered specific capacity of 1180, 1100, 1040, 910, and 710 mA h g^{-1} at

Research Article
doi.org/10.1002/batt.202500485
Chemistry Europe
European Chemical Societies Publishing

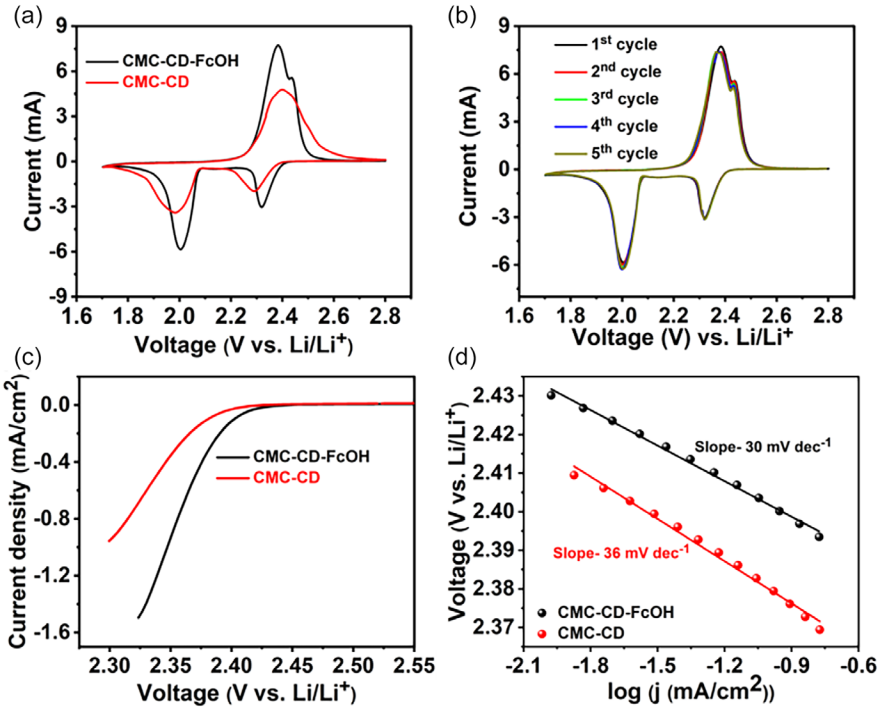

Figure 2. a) CV profile of CMC-CD and CMC-CD-FcOH (at 0.1 mV s^{-1}), b) CV profile of CMC-CD-FcOH, c) plot of V versus current density (derived from CV profile), and d) Tafel plot cathodic peak.

0.1, 0.2, 0.5, 1, and 2 C, respectively (**Figure 3**a). Upon switching the C rate to 0.1 the cell could retain 1180 mA h g^{-1}. On the other hand, the LSBs with CMC-CD could deliver 980, 830, 740, 600 and 405 mA h g^{-1} at 0.1, 0.2, 0.5 1, and 2 C, respectively. Upon switching the C rate to 0.1 the cell could reach a specific capacity of 950 mA h g^{-1}. The higher specific capacity and capacity retention for CMC-CD-FcOH compared to CMC-CD is attributed to its better polysulfide immobilization capabilities and faster

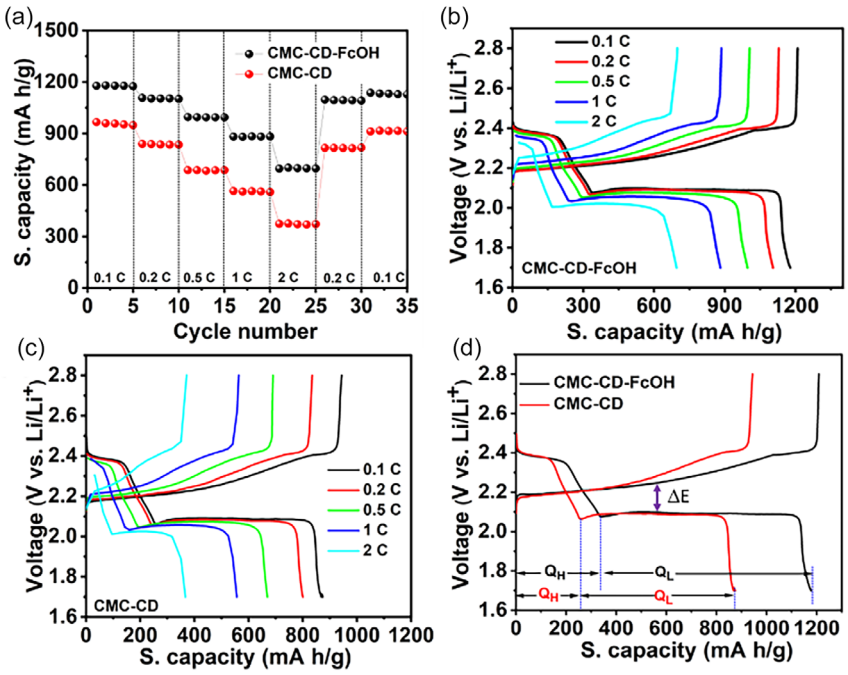

Figure 3. a) Rate capability test for LSBs with CMC-CD-FcOH and CMC-CD, galvanostatic charge–discharge (GCD) profiles at different C rates for LSBs with b) CMC-CD-FcOH, c) CMC-CD, and d) plot of GCD profile at 0.1 C.

Research Article
doi.org/10.1002/batt.202500485
Chemistry Europe
European Chemical Societies Publishing

conversion kinetics. The corresponding charge–discharge profiles for LSBs with CMC-CD-FcOH and CMC-CD are shown in the Figure 3b,c respectively. The charge–discharge profiles at 0.1 C shows a typical two-step reduction process at 2.4 and 2.1 V, which matches with the CVs. The polarization potential (ΔE) is lower for the cells with CMC-CD-FcOH (133 mV) compared to that of CMC-CD (152 mV), which again highlights that the polysulfide conversion rate is faster in the case of the former cathode (Figure 3d). Furthermore, the ratio of the capacities at low plateau (Q_L) and the high plateau (Q_H) region is higher in the case of LSBs with CMC-CD-FcOH (2.5) when compared to that with CMC-CD (2.25). This indicates that the kinetics of polysulfide conversion are faster in the case of CMC-CD-FcOH compared to that with CMC-CD (Figure 3d).

The long-term cycling tests were then conducted to understand the influence of the binders on the stability of LSBs. The cells were initially tested at 0.2 C, the LSBs with CMC-CD-FcOH delivered an initial specific capacity of 1075 mA h g^{-1} and could retain nearly 89% of their initial capacity after 120 cycles (**Figure 4**a). On the other hand, the LSBs with CMC-CD showed 1070 mA h g^{-1} at 0.2 C and could retain ≈75% of its initial capacity after 120 cycles. The observed difference of 14% in the capacity and capacity retention is attributed to the strong polysulfide adsorption energy and their conversion kinetics in case of CMC-CD-FcOH. This is attributed to Lewis acidic–basic interaction between polysulfides and Fe^{2+} center of FcOH. Considering the improved electrochemical performance of LSBs with CMC-CD-FcOH, the batteries were tested at 0.5 and 1 C rates. At 0.5 C, the LSBs displayed an initial specific capacity of 1035 mA h g^{-1} and after 500 cycles, the cell could retain nearly 75% of its initial capacity (Figure 4b). The corresponding charge–discharge profile at 0.5 C is shown in Figure 4c. At 1 C, the cell could deliver an initial capacity of 970 mA h g^{-1} and retained 700 mA h g^{-1} at the end of 250th cycle (Figure 4d). Thus, even at higher C rates, the cells were stable for several hundreds of charge–discharge cycles. Although the polysulfide dissolution has been suppressed to a significant extent, the coulombic efficiency data indicate that the dissolution is not completely suppressed. Furthermore, the batteries were tested at practically relevant lean electrolyte conditions (E/S ratio of 5 μL mg^{-1}). The LSBs with sulfur loading of 3.8 mg cm^{-2} under lean electrolyte condition delivered an initial capacity of 900 mA h g^{-1} at 1 C and could retain ≈70% of its initial capacity at the end of the 50th cycle. Similarly, the cell with 4.7 mg cm^{-2} sulfur-loaded cathode delivered 780 m Ah g^{-1} and retained ≈500 mA h g^{-1} after 50 cycles (Figure 4e). Thus, even at practically relevant conditions, the batteries delivered good performance.

To understand the kinetics of Li-ion diffusion and polysulfide conversion at the electrode–electrolyte interface the electrochemical impedance analysis was carried out. The Nyquist plot displayed a single semicircle at the initial stage for both CMC-CD and CMC-CD-FcOH. The cell comprising CMC-CD possessed a higher charge transfer resistance (R_{ct}) compared to that of CMC-CD-FcOH (Figure 4f). After 100 cycles, the cells displayed two semicircles: one in the high-mid frequency region, corresponding to the resistance from the residual polysulfides (R_o) and a semicircle in the low frequency region corresponds to the R_{ct} (Figure 4f). The cell comprising CMC-CD-FcOH displayed lower R_o and R_{ct} values compared to those of CMC-CD. This is attributed to the faster Li-ion diffusion and stronger polysulfide immobilizing capabilities of CMC-CD-FcOH compared to that of CMC-CD. To understand the structural stability

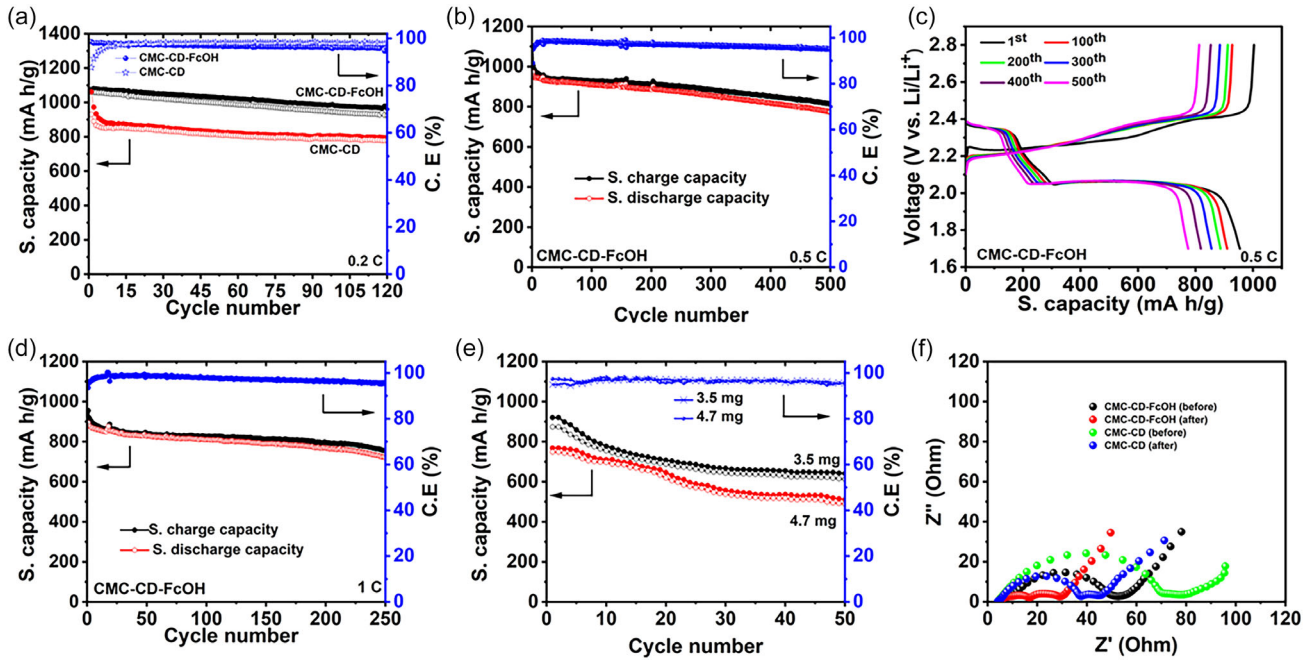

Figure 4. a) cyclic stability of CMC-CD and CMC-CD-FcOH (0. 2 C), b) cyclic stability of CMC-CD-FcOH at 0.5 C, c) GCD profile of CMC-CD-FcOH at 0.5 C, and d) cyclic stability of CMC-CD-FcOH at 1 C. e) Cyclic stability of LSB (CMC-CD-FcOH) at 1 C with different sulfur loading and f) electrochemical impedance spectroscopy (EIS) profile of LSBs with CMC-CD and CMC-CD-FcOH before and after cycling.

and the interactions between the polymer binder and the LiPSs, the pre- and postcycling X-ray photoelectron spectroscopy (XPS) and field emission scanning electron microscopy (FESEM) images of the electrodes were recorded. The as prepared electrodes' XPS of Ni2p and Fe2p spectra are shown in (Figure S8, Supporting Information). The Fe2p spectrum showed characteristic Fe^{2+} peaks at 708 and 714 eV, respectively, with a satellite shoulder at 714 and 723 eV (Figure S8a, Supporting Information). Similarly, the Ni2p spectra showed characteristic Ni^{2+} peaks at 856 and 873 eV, respectively, with satellite shoulders at 865 and 881 eV (Figure S8b, Supporting Information). The postcycling C1s spectrum showed the presence of Fe–C, C–O, peaks corresponding the CMC-CD-FcOH complex, while the peaks C—N, —C═O, —(C═O) O, and —C—F are electrolyte-derived products (Figure S9a, Supporting Information).[37] Similarly, the O1s spectrum showed the presence of —C—O—Li peak at 532 eV (Figure S9b, Supporting Information).[38] The Ni2p spectrum showed the presence of Ni (0) peak around 850 eV, indicating an electron transfer from Ni^{2+} to LiPSs, which is further revealed by the presence of Ni—S peak around 853 eV (Figure S9c, Supporting Information).[39] This shows that Ni^{2+} of NPT showed strong electrostatic interactions between polysulfides. The Fe 2p spectrum also showed the presence of Fe (0) peak around 700 eV indicating an electron transfer to LiPSs which was further confirmed by Fe—S peak around 708 eV (Figure S9d, Supporting Information).[40] This further highlights the strong interaction between Fe^{2+} of ferrocene with LiPSs. The Li1s spectrum showed the presence of Li—O and Li—S peaks, which are attributed to the interactions between the —OH groups and the LiPSs (Figure S9e, Supporting Information). The S2p spectrum revealed the presence of LiPSs, sulfonate, and polythionate peaks at 164, 167, and 168.5 eV, respectively (Figure S9f, Supporting Information).[41] To understand the films' morphology, we dismantled the batteries and imaged the cathode surface. For comparison, we also imaged the surface of the cathode before charge–discharge experiment. The FESEM images of cathodes don't show any significant difference between the cells comprising CMC-CD-FcOH and CMC-CD. It is interesting to note that the cracks didn't appear in electrodes that were subjected to charge–discharge cycling (Figure S8, Supporting Information). We did observe cracks in batteries prepared using PVDF as binder.[42] Furthermore, cathode electrolyte interface formed on the electrode with CMC-CD-FcOH doesn't show voids that are found in the one based on CMC-CD. We attribute this to the probable polysulfide films formed between Fe^{2+} and polysulfides.

3. Conclusion

Water-soluble polymer sodium salt of CMC was chosen to be the binder along with CD. The 21 hydroxyl moieties of CD formed hydrogen bonding with the carbonyl moieties of CMC, resulting in a mechanically robust polymeric binder. The modulus of 64.3 MPa corroborates the mechanical robustness of the film. The CD is used to form an inclusion complex with FcOH. The Fe^{2+} in FcOH is a Lewis acid that attracted the Lewis basic polysulfides and suppressed the polysulfide dissolution. The binder also comprises nickel phthalocyanine that electro catalyzes the sulfur redox reaction. The binder with inclusion complex showed well defined redox peaks in the anodic and cathodic scans, indicating the efficient conversion of sulfur to polysulfides. The lower current density of absence of two peaks during the formation of S_8 in the binder that doesn't have an inclusion complex corroborate the role of Fe^{2+} in redox process. The Li–S batteries with inclusion complex suppressed polysulfide dissolution, hence those batteries showed cycling stability over 500 charge–discharge cycles. The Li–S batteries with high sulfur loading (4.7 mg cm^{-2}) and lean electrolyte (E/S of 5 μL mg^{-1}) delivered a specific capacity of 780 mA h g^{-1}.

Acknowledgements

K.K. thank Aeronautics Research and Development Board (2010) for funding. H.J.B. thanks UGC, India for fellowship.

Conflict of Interest

The authors declare no conflict of interest.

Data Availability Statement

The data that support the findings of this study are available from the corresponding author upon reasonable request.

Keywords: carboxy methyl cellulose · cyclodextrin · ferrocene methanol · Li–S batteries

[1] S. Chung, A. Manthiram, *Adv. Mater.* **2019**, *31*, 1901125.
[2] A. Manthiram, Y. Fu, Y.-S. Su, *Acc. Chem. Res.* **2013**, *46*, 1125.
[3] T. Li, X. Bai, U. Gulzar, Y.-J. Bai, C. Capiglia, W. Deng, X. Zhou, Z. Liu, Z. Feng, R. P. Zaccaria, *Adv. Funct. Mater.* **2019**, *29*, 1901730.
[4] H. Duan, K. Li, M. Xie, J.-M. Chen, H.-G. Zhou, X. Wu, G.-H. Ning, A. I. Cooper, D. Li, *J. Am. Chem. Soc.* **2021**, *143*, 19446.
[5] C. Zhou, M. Li, N. Hu, J. Yang, H. Li, J. Yan, P. Lei, Y. Zhuang, S. Guo, *Adv. Funct. Mater.* **2022**, *32*, 2204635.
[6] G. Zhou, H. Chen, Y. Cui, *Nat. Energy* **2022**, *7*, 312.
[7] W. Bao, L. Liu, C. Wang, S. Choi, D. Wang, G. Wang, *Adv. Energy Mater.* **2018**, *8*, 1702485.
[8] X.-B. Cheng, R. Zhang, C.-Z. Zhao, Q. Zhang, *Chem. Rev.* **2017**, *117*, 10403.
[9] K. C. Ranjeesh, B. H. Javaregowda, S. Gaber, P. Bhauriyal, S. Kumar, T. Skorjanc, M. Finšgar, T. Heine, K. Krishnamoorthy, D. Shetty, *Adv. Sci.* **2025**, *12*, 2415897.
[10] G. Zhou, L.-C. Yin, D.-W. Wang, L. Li, S. Pei, I. R. Gentle, F. Li, H.-M. Cheng, *ACS Nano* **2013**, *7*, 5367.
[11] B. Du, Y. Luo, Y. Yang, W. Xue, G. Liu, J. Li, *Chem. Eng. J.* **2022**, *442*, 135823.
[12] B.-J. Lee, C. Zhao, J.-H. Yu, T.-H. Kang, H.-Y. Park, J. Kang, Y. Jung, X. Liu, T. Li, W. Xu, X.-B. Zuo, G.-L. Xu, K. Amine, J.-S. Yu, *Nat. Commun.* **2022**, *13*, 4629.
[13] F. Chu, M. Wang, J. Liu, Z. Guan, H. Yu, B. Liu, F. Wu, *Adv. Funct. Mater.* **2022**, *32*, 2205393.
[14] R. Soni, D. Spadoni, P. R. Shearing, D. J. L. Brett, C. Lekakou, Q. Cai, J. B. Robinson, T. S. Miller, *ACS Appl. Energy Mater.* **2023**, *6*, 5671.
[15] Y.-H. Liu, L.-X. Li, A.-Y. Wen, F.-F. Cao, H. Ye, *Energy Storage Mater.* **2023**, *55*, 652.
[16] H. Chen, M. Ling, L. Hencz, H. Y. Ling, G. Li, Z. Lin, G. Liu, S. Zhang, *Chem. Rev.* **2018**, *118*, 8936.

[17] Q. Gong, L. Hou, T. Li, Y. Jiao, P. Wu, *ACS Nano* **2022**, *16*, 8449.
[18] M. A. Spreafico, P. Cojocaru, L. Magagnin, F. Triulzi, M. Apostolo, *Ind. Eng. Chem. Res.* **2014**, *53*, 9094.
[19] D. Bresser, D. Buchholz, A. Moretti, A. Varzi, S. Passerini, *Energy Environ. Sci.* **2018**, *11*, 3096.
[20] H. Wang, P. Zheng, H. Yi, Y. Wang, Z. Yang, Z. Lei, Y. Chen, Y. Deng, C. Wang, Y. Yang, *Macromolecules* **2020**, *53*, 8539.
[21] B. Jin, Y. Li, J. Qian, X. Zhan, Q. Zhang, *ChemElectroChem* **2020**, *7*, 4158.
[22] Q. Lemarié, F. Alloin, P. X. Thivel, H. Idrissi, L. Roué, *Electrochim. Acta* **2019**, *299*, 415.
[23] M. Shaibani, M. S. Mirshekarloo, R. Singh, C. D. Easton, M. C. D. Cooray, N. Eshraghi, T. Abendroth, S. Dörfler, H. Althues, S. Kaskel, A. F. Hollenkamp, M. R. Hill, M. Majumder, *Sci. Adv.* **2025**, *6*, eaay2757.
[24] M.-K. Song, Y. Zhang, E. J. Cairns, *Nano Lett.* **2013**, *13*, 5891.
[25] S. Waluś, A. Robba, R. Bouchet, C. Barchasz, F. Alloin, *Electrochim. Acta* **2016**, *210*, 492.
[26] Y. Huang, M. Shaibani, T. D. Gamot, M. Wang, P. Jovanović, M. C. D. Cooray, M. S. Mirshekarloo, R. J. Mulder, N. V. Medhekar, M. R. Hill, M. Majumder, *Nat. Commun.* **2021**, *12*, 5375.
[27] M. M. Nishshanke, P. Jovanović, M. R. Panda, M. J. Abedin, D. McNamara, M. R. Hill, J. Bhattacharya, C. Kamal, M. Shaibani, M. Majumder, *Adv. Energy Mater.* **2025**, *15*, 2403092.
[28] Y. X. Ren, T. S. Zhao, M. Liu, Y. K. Zeng, H. R. Jiang, *J. Power Sources* **2017**, *361*, 203.
[29] Y. Tsao, M. Lee, E. C. Miller, G. Gao, J. Park, S. Chen, T. Katsumata, H. Tran, L.-W. Wang, M. F. Toney, Y. Cui, Z. Bao, *Joule* **2019**, *3*, 872.
[30] J. B.H., B. R. Shivankar, S. Krishnamurty, D. Chen, R. A. Caruso, K. Krishnamoorthy, *Catal. Sci. Technol.* **2024**, *14*, 3416.
[31] W. Huang, Z. Lin, H. Liu, R. Na, J. Tian, Z. Shan, *J. Mater. Chem. A* **2018**, *6*, 17132.
[32] H.-J. Schneider, F. Hacket, V. Rüdiger, H. Ikeda, *Chem. Rev.* **1998**, *98*, 1755.
[33] Q. Zou, Y.-C. Lu, *J. Phys. Chem. Lett.* **2016**, *7*, 1518.
[34] Z. Ma, H. Wu, Y. Wang, Y. Pan, C. Lu, *Int. J. Plast.* **2017**, *88*, 188.
[35] Y. Wang, Y. Pu, Z. Ma, Y. Pan, C. Q. Sun, *Extreme Mech. Lett.* **2016**, *9*, 226.
[36] G. X. Dong, Y. Wang, W. J. Jiang, Y. L. Zou, Z. S. Ma, *Sci. China Technol. Sci.* **2022**, *65*, 1798.
[37] J. Zhang, J. Yang, Z. Liu, B. Zheng, *ACS Omega* **2021**, *6*, 4995.
[38] J. Liu, Y. Zhou, Z. Xiao, M. Xue, S. Liu, T. Yan, *Chem. Eng. J.* **2024**, *484*, 149596.
[39] P. Xia, W. Lei, X. Wang, Z. Luo, Y. Pan, Z. Ma, *J. Alloys Compd.* **2020**, *832*, 153692.
[40] L. Zhou, H. Li, Y. Zhang, M. Jiang, D. L. Danilov, R.-A. Eichel, P. H. L. Notten, *Mater. Today Commun.* **2021**, *26*, 102133.
[41] L. Zhang, D. Liu, Z. Muhammad, F. Wan, W. Xie, Y. Wang, L. Song, Z. Niu, J. Chen, *Adv. Mater.* **2019**, *31*, 1903955.
[42] C. Li, Q. Sun, Q. Zhang, C. Xu, S. Wang, Y. Ma, X. Shi, H. Zhang, D. Song, L. Zhang, *Chem. Eng. J.* **2023**, *455*, 140706.

Manuscript received: June 26, 2025
Revised manuscript received: August 20, 2025
Version of record online: